separations

MDPI

Article

Spatially and Temporally Resolved Analysis of Bleeding in a Centrifugal Partition Chromatography Rotor

Felix Buthmann, Philip Laby, Djamal Hamza, Jörg Koop and Gerhard Schembecker *

Laboratory of Plant and Process Design, Department of Biochemical and Chemical Engineering, TU Dortmund University, 44227 Dortmund, Germany

* Correspondence: gerhard.schembecker@tu-dortmund.de; Tel.: +49-(0)231-755-2339

Abstract: Centrifugal Partition Chromatography (CPC) is a separation technique that utilizes immiscible liquid phases to purify compounds. The selection of solvents in Liquid–Liquid Chromatography offers flexibility and optimization possibilities for specific separation tasks. Understanding the hydrodynamics inside the apparatus is crucial for optimizing a CPC process. The phase retention ratio (*Sf*) determines the apparatus's operating point and separation efficiency. However, stationary phase leakage, known as bleeding, complicates the immobilization of this phase. We used a partly transparent single-disc rotor to investigate the time and space dependency of bleeding inside a CPC apparatus, enabling real-time and localized determination of the phase retention ratio. By tracking the retention values over time, we observed the bleeding phenomenon and its progression from the inlet to the rotor outlet. Depending on the phase system used, the CPC was utilizable for a separation task for only 173–500 dimensionless residence times. Systems with a higher stability parameter (as described in the literature) showed a lower bleeding rate and increased stability over time. Accordingly, our results demonstrate the importance of maintaining an optimal ratio of mobile to stationary phase for efficient separation.

Keywords: Centrifugal Partition Chromatography; stationary phase retention; bleeding; transparent rotor design; flow regime measurement

Citation: Buthmann, F.; Laby, P.; Hamza, D.; Koop, J.; Schembecker, G. Spatially and Temporally Resolved Analysis of Bleeding in a Centrifugal Partition Chromatography Rotor. *Separations* **2024**, *11*, 56. https://doi.org/10.3390/separations11020056

Academic Editor: Beatriz Albero

Received: 18 January 2024
Revised: 5 February 2024
Accepted: 8 February 2024
Published: 10 February 2024

1. Introduction

In Liquid–Liquid Chromatography, two immiscible phases are used as mobile and stationary phases. This implies several advantages, such as the wide range of usable solvents, resulting in the possibility of tailor-made, highly optimized processes for a given separation task [1–6]. In this context, models for solvent selection were developed, allowing for a sophisticated choice of fluids [7–12]. Furthermore, liquid stationary phase costs are commonly less than solid material costs [1]. In Centrifugal Partition Chromatography (CPC), a rotor spinning around a central axis is used to immobilize the stationary phase. At high *g*-forces, the latter is entrapped inside a cascade of chambers and ducts on the rotor disc [13,14]. The first prototype of this apparatus was built by Murayama in early 1982 [15]. From thereon, publications on CPC increased continuously, showing the growing interest in this topic (Figure A1).

Besides the sample properties, the partition coefficient K_D and physical properties (viscosity, interfacial tension, densities, wettability) of the solvent system affect the efficiency of the chromatograph [16,17]. The third parameter group influencing the separation is operating conditions (e.g., volume flow, rotational speed, operation mode).

All three groups of parameters severely impact hydrodynamics inside the apparatus [18]. This leads to different flow regimes evolving, which have been well characterized in the literature [19–23].

As mentioned, CPC is capable of realizing complex separation tasks—for example, when it comes to the isolation of 10-Deacetyl Baccatin III, an intermediate in the semisynthetic production of the chemotherapy drug taxol, or the separation of cannabinoids from

Cannabis sativa L extract [24,25]. An optimal chromatographic resolution is crucial for those separations, leading to baseline-separated peaks and, therefore, high yield and purity of the target compound. In this context, the direct link between the chromatographic resolution and the amount of stationary phase (V_{stat}) immobilized inside the rotor is known in the literature and is summarized in the following. The stationary phase retention is characterized with the help of the phase retention ratio *Sf* [13].

$$Sf = \frac{V_{stat,chamber} + V_{stat,duct}}{V_{chamber} + V_{duct}} \quad (1)$$

The normalized phase retention ratio *Sf** compensates for different rotor geometries [19,26].

$$Sf^* = \frac{Sf}{Sf_{max}} \text{ with } Sf_{max} = \frac{V_{chamber}}{V_{chamber} + V_{duct}} \quad (2)$$

This relation is depicted in Figure 1. For components with a $K_D < 1$, the retention volume (V_R) and the retention time (t_R) increase with decreasing *Sf*. In contrast, V_R decreases with decreasing *Sf* for components with a $K_D > 1$ [13]. The phase retention is critical for a separation task aiming to separate a component A with a $K_D = 2$ from a component B with a $K_D = 0.1$. A chromatographic plant with a low *Sf* value of 0.1 can not separate these components with high efficiency because the retention times would resemble one another (9 min vs. 11 min, cf., solid arrows in Figure 1). The resulting chromatographic peaks would overlap, and the corresponding resolution would be low. The same plant would separate both components with a high efficiency when operated with a phase retention of 0.6. In this case, the corresponding retention times would be 5 min and 19 min (dashed arrows in Figure 1), implying baseline-separated peaks and, therefore, a sufficient resolution. Consequently, phase retention is a crucial parameter to investigate when optimizing separation efficiency in Centrifugal Partition Chromatography. Aggravating this, the immobilization of the stationary phase inside the apparatus is not ideal: the stationary phase leaks out of the chromatograph during operation, the so-called bleeding. Bleeding is caused by imperfect coalescence of the mobile phase at the outlet of each chamber inside the rotor. After being dispersed in the stationary phase initially, the mobile phase coalesces (boosted by centrifugal force). Nevertheless, droplets of the stationary phase remain in this coalescence zone and elute with the mobile phase flow [13,19,27]. Consequently, the resolution decreases over time, which cuts productivity.

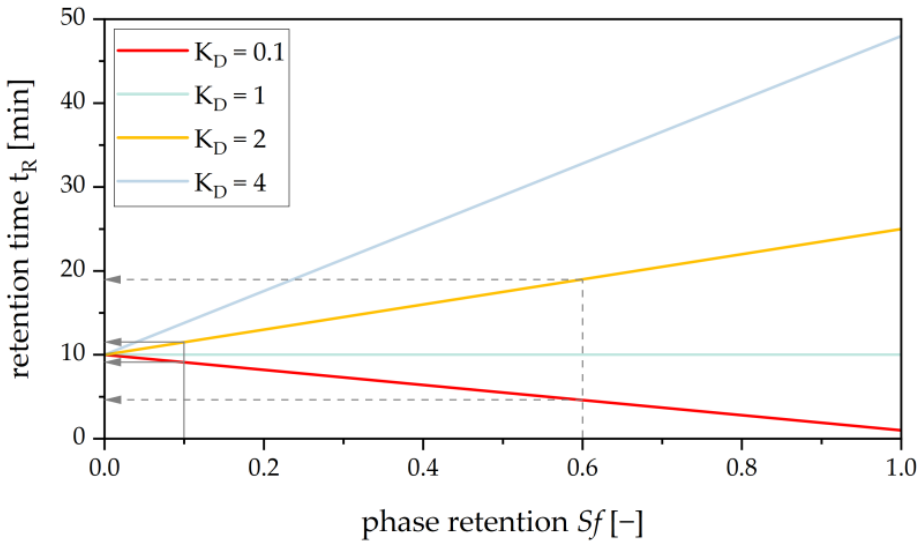

Figure 1. Retention time over proportion of stationary phase/retention (*Sf*) inside a CPC apparatus for different K_D values.

As stated by Berthod, "CPC should be compared to preparative Liquid Chromatography (LC) only" [13]. CPC is not able to perform analytical chromatography, as samples in the range of only several microlitres cannot be processed. Regarding preparative separation tasks, the operating ranges of LC and CPC differ: CPC works at comparatively small plate numbers along with high phase ratios ($V_{stationary\ phase} \cdot V_{mobile\ phase}^{-1}$). On the other hand, LC can reach high plate numbers but is limited in the phase ratio [13]. In conclusion, CPC and LC should be seen as complementary techniques rather than direct competitors.

This work aims to gain spatially and temporally resolved understanding of the retention in a CPC rotor for different biphasic systems. It has to be proved whether bleeding occurs in all chambers of the rotor simultaneously or whether stationary phase loss happens in the first chambers of the rotor initially before this front of bleeding consecutively impacts more and more chambers downstream. With the help of this knowledge, optimization of separation tasks concerning productivity will be possible, and even adapted operation modes are conceivable. To achieve this, a partly transparent rotor is used [28,29].

In the first experimental step, flow regime maps for all liquid–liquid systems investigated have to be recorded to ensure a constant flow regime during all experiments. Because of deviating physical properties (especially viscosity, η, interfacial tension, γ, and density, ρ), the volumetric flow rate of the mobile phase necessary for optimal operation of the different systems differs. Based on this optimal volumetric flow rate, spatially and temporally resolved retention measurements will be performed afterward. Mobile phase temperatures during the retention experiments will be measured simultaneously to estimate the impact of energy input from the pumps and rotary joints on the system's miscibility gap.

2. Materials and Methods

2.1. Centrifugal Partition Chromatograph with Transparent Rotor

The rotor used in this study is a single-disc rotor with a cascade of chambers and ducts (Sf_{max} = 0.782, V_{rotor} = 10.4 mL). Their geometry is based on the FCPC design and has been examined and optimized in previous publications [14,30–32]. In contrast to larger setups with stacked rotors for preparative separation tasks, images of this single-disc rotor disc can be obtained with the help of a triggered monochromatic camera (AccuPIXEL© TM 1327GE from Jai Pulnix, Yokohama, Japan) and an LED-flash (wavelength 627 nm, type CCS TH 63X60RD from Stemmer Imaging, Puchheim, Germany). This rotor has six viewing windows—enabling visual inspection of approximately 50% of the chambers (66 chambers in total). The setup is mounted inside the chromatograph (FCPC, Chromaton, Annonay, France), as shown in Figure 2.

The electric motor can provide 200 to 2000 rounds per minute. The chromatograph was operated at 750 rpm for all experiments to avoid high wear. When triggered once per revolution, the light barrier sends a signal to a controller (RT420cc, Gardasoft, Cambridge, UK). After an adjustable delay, this control unit simultaneously actuates the LED flash and the monochromatic camera. For different rotation speeds, various delays are programmed. Raw data is sent to a Labview instance (Labview 2020, National Instruments, Austin, TX, USA). The script automatically collects images in one video per viewing window. The data acquisition is controlled, so videos are saved in an adjustable time interval. Two rotary joints are necessary to establish a continuous fluid flow inside the chambers and ducts of the spinning rotor. Those mechanical components ensure a tight seal between non-rotating capillaries from the pumps and rotating capillaries connected directly to the rotor itself (cf., Figure 1). Two identical pumps (Azura P2.1S, Knauer, Berlin, Germany) are installed.

Based on previous research and the technical limits of the components, volume flows between 2.5 and 40 mL·min^{-1} were chosen to ensure a highly dispersed flow regime across all phase systems used [16,33,34]. The experiments were performed at 22 °C.

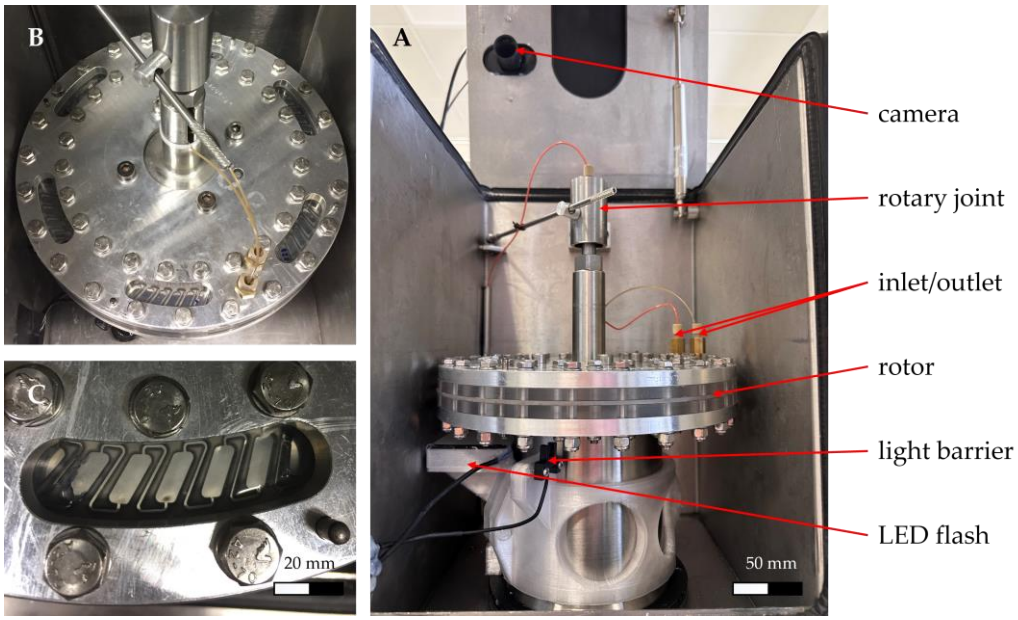

Figure 2. (**A**) CPC assembly: The rotor is flanged to an electric motor with an upright rotation axis. Two rotary joints (the lower one not shown) ensure fluid flow from the inlet to the outlet. The light barrier is triggered once per revolution, whereby an LED flash and a camera are actuated. (**B**) Top view of the rotor with six viewing windows. (**C**) The first viewing window with four chambers and interconnecting ducts is completely visible.

2.2. Phase System

The Arizona family was used as the phase system, containing methanol (99%), ethyl acetate (99.9%), heptane (99.8%) (all supplied by VWR International, Radnor, PA, USA), and water purified by a MILLI-Q® system (Millipak® Express 40, Merck, Darmstadt, Germany). The selected systems of the Arizona family are shown in Table 1.

Table 1. Composition of the Arizona family [17].

Arizona System	Heptane vol%	EtAc vol%	MeOH vol%	Water vol%
A	0	50	0	50
...	...	...	...	...
G	10	40	10	40
...	...	...	...	...
N	25	25	25	25
...	...	...	...	...
U	40	10	40	10
...	...	...	...	...
Z	50	0	50	0

The phase systems Arizona G, N, and U were examined due to their white spread in polarity (physical data can be found in Table A1). Because of being prone to hydrolysis, all systems were prepared and used within 24 h [35]. After initial mixing, a settling time of 1 h for every 1 L batch was ensured. All systems were stored in a water bath (22 °C) before and during the experiments. Aqueous and organic phases stayed in contact to maintain thermodynamic equilibrium. The tubing towards the pumps was placed centrally in the respective phase. To enhance the contrast between the liquids, the aqueous phase was dyed with methylene blue (20 mg/L of heavy phase, Merck, Darmstadt, Germany), having no impact on the liquid–liquid equilibrium and physical properties, as shown by Fromme [19].

The rotor was initially filled with the light phase for all experiments to prepare for a measurement. Then, switching the mobile flow to the heavy phase marked the start of each

experiment (meaning operation in descending mode). This was carried out with the help of a valve.

The mobile phase was pumped through the rotor for 10 dimensionless hydrodynamic residence times before a video was taken to examine the dispersion state. The procedure was repeated for volume flows between 2.5 and 40 mL·min^{-1} (technical limits of the apparatus).

The retention analysis was performed analogously: after the same initial procedure, the normalized retention value, *Sf**, was determined based on the videos taken at intervals of 10 min. This procedure was repeated until the *Sf** approached zero, meaning no light phase was left inside the rotor. The flow rate of the mobile phase was determined according to the initial dispersion state experiments.

To track the energy input from the pumps and rotary joints, the temperature of the mobile phase at the outlet was measured (Pt100 sensor, Heinz GmbH, Elgersburg, Germany). All experiments were performed in triplicate.

2.3. Retention Evaluation

For the determination of retention values from the video files, an optimized code based on our previous work was used [36]. Since the two-dimensional profile of the chamber geometry is known, it is directly localizable in the images captured. Therefore, the entire profile is searched instead of identifying individual chambers to ensure the most precise detection. This approach enables a reproducible analysis of retention on a single-chamber basis, and the algorithm provides even more detailed information than its predecessor, which was capable of analyzing a viewing window (4 chambers). The subsequent area recognition and calculation of *Sf** are performed using the previous methods. This adapted image evaluation process is shown in Figure A2 and described in detail below.

An image extracted from the raw video files undergoes initial edge detection (analogous to [36]). In a second novel step, a template is generated from the computer-aided design of the rotor and rasterized over the raw data image. The template is iteratively shifted in the x and y directions, and the correspondence between the two images is calculated. This process is repeated for rotation angles from -5.3° to 5.3° in 0.1° increments. Analysis of larger rotation angles is unnecessary, as 5.3° corresponds to the angle between two adjacent chambers. Image congruence is calculated by multiplying the values of overlapping pixels and summing their results. The parameter set that yields the highest sum is stored as the optimum. The computation process is accelerated using discrete Fourier transformations. Based on the values for translation and rotation angles for the optimum, the corresponding image areas of the chambers and channels are monochromatized, and the number of white pixels is counted to determine the area fraction of the uncolored phase. This enables the final calculation of the *Sf** value for each combination of a chamber and its downstream channel, following the routine described [36].

3. Results and Discussion

3.1. Flow Regime Measurements

The qualitative analysis of flow regimes was performed for mobile phase flows between 2.5 and 40 mL·min^{-1}, with a resolution of 2.5 mL·min^{-1}. For a detailed analysis, the flow regimes for different phase systems in the rotor's first, third, and last inspection window are listed in Figures A3–A5. Results for the optimal volume flows chosen are shown in Figure 3.

As the literature describes, different flow regimes are apparent in Centrifugal Partition Chromatography [19,34,37]. An undispersed regime occurs at low volume flows for Arizona N, where the mobile phase mainly flows next to the chamber's walls (as shown in Figure A3). This behavior is evident at 2.5 and partly 5 mL·min^{-1} flow rates.

Between 7.5 and 10 mL·min^{-1}, a low dispersed state can be observed for this phase system. Here, a lamella of the mobile phase flows into the chamber, and droplet breakup is only apparent near the phase boundary of the stationary phase.

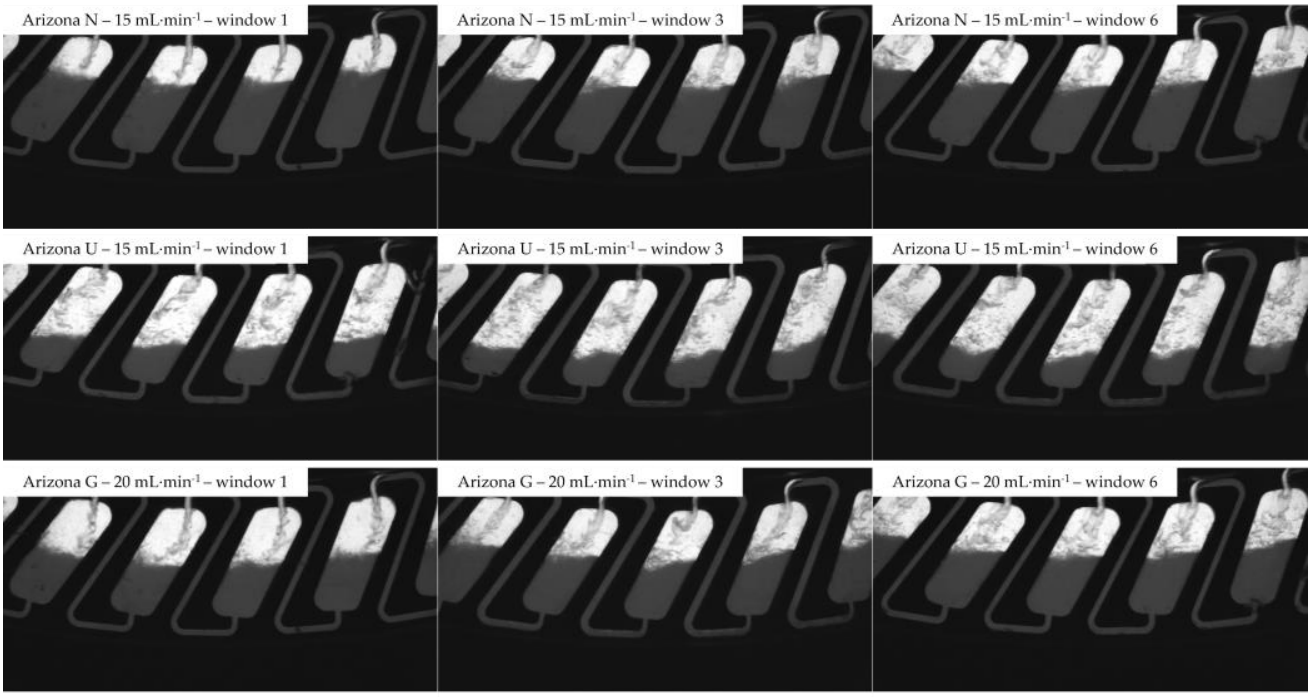

Figure 3. Hydrodynamics with a constant flow regime for different phase systems after 10 dimensionless hydrodynamic residence times. Phase system used: Arizona N, U, and G, 22 °C, FCPC single-disc rotor, desc. mode, 750 rpm.

Starting at 12.5 mL·min^{-1}, a transition to a highly dispersed flow regime occurs, corresponding to a lamella breakup next to the inlet duct—leading to more droplet formation and increased interfacial area. This flow regime is a good trade-off between maximized mass transfer (mobile to stationary phase and vice versa) and a low bleeding rate [34]. At volumetric flow rates of 22.5 mL·min^{-1} and higher, the mobile phase can be characterized as atomized. The formation of droplets takes place immediately after the inflowing duct. As mentioned, bleeding is promoted at those high mobile phase flow rates. The amount of undyed stationary phase is remarkably lower at 40 than at 20 mL·min^{-1}, and the bleeding rate is comparably high.

For the following retention experiments, 15 mL·min^{-1} was chosen as the volumetric flow rate for Arizona N, as the favored highly dispersed flow regime is formed here. At the same time, no signs of an atomized regime are evident.

For Arizona U, similar can be stated. The flow regime map (Figure A4) is comparable to Arizona N, with a minor shift towards higher volume flows. Keeping the volume flow at 15 mL/min ensures a highly dispersed flow regime.

With Arizona G, on the other hand, the higher dispersed regimes shift significantly towards higher volume flows (Figure A5). The transition towards the highly dispersed state is reached at 17.5 mL·min^{-1}. Therefore, 20 mL·min^{-1} was chosen as the mobile phase flow.

These volumetric flow rates (Figure 3) for the different phase systems ensure a constant flow regime for all of the following retention experiments. In conclusion, all results regarding hydrodynamics in the rotor should be comparable.

3.2. Retention Measurements

The measurement of *Sf** over time for Arizona N (equal vol% of all components) and a volume flow of 15 mL·min^{-1} is shown in Figure 4.

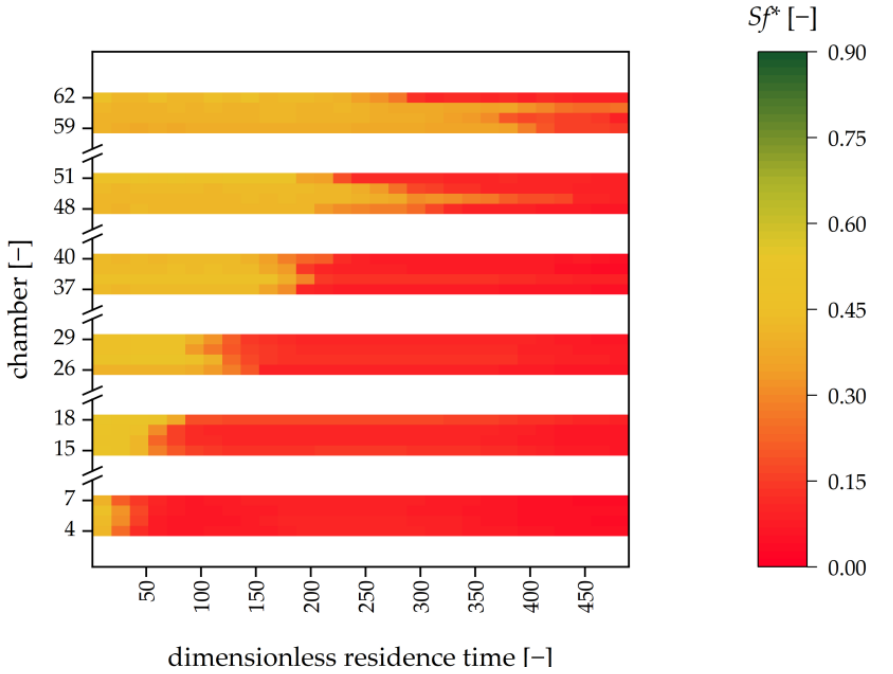

Figure 4. Retention values over time for the 6 viewing windows (containing 4 chamber–duct combinations each) of a transparent single-disc rotor. White areas indicate intransparent regions of the rotor. Phase system used: Arizona N, mobile phase flow: 15 mL·min^{-1}, 22 °C, 750 rpm, tripled runs.

As mentioned, the volumetric flow rate was set to 15 mL·min^{-1}. The dimensionless residence time is calculated based on the hydrodynamic residence time being 0.69 min for the given setup. The heatmap shows that all inspection windows start with retention values between 0.42 and 0.46. From this value, the first inspection window (chambers 4–7) loses stationary phase quickly, resulting in a mean Sf^* of 0.15 after 43 dimensionless residence times only. This equals a loss of 0.035 mL of stationary phase during this time, being 65.5% of the amount of stationary phase present in inspection window 1 after 10 min (14 dimensionless residence times). A similar trend is apparent for the second inspection window (chambers 15–18). The loss of stationary phase (74.8%) is in a comparable range but shifted timewise: the collapse of Sf^* starts at 43 dimensionless residence times. This behavior persists throughout the following chambers, leading to the last viewing window 6, where major bleeding is apparent after 375 dimensionless residence times.

For sufficient separation efficiency, the amount of stationary phase in the system is critical (cf., Figure 1). Therefore, according to literature data, Sf between 0.2 and 0.8 must be maintained (depending on the separation task) [13]. With the mean Sf^* for the entire rotor being 0.251 after 120 min (173 dimensionless residence times), a separation would not be advisable after two hours of operation.

For Arizona U, a similar trend is visible (Figure 5). The first inspection window (chambers 4–7) bleeds stationary phase after 29 dimensionless residence times.

The initial retention value for this system is between 0.71 and 0.86. After 60 min (86 dimensionless residence times), 0.062 mL of stationary phase is lost in the first inspection window, which equals a proportion of 74.2%. Compared to Arizona N, the same trend is evident, but bleeding starts later. The loss in the second inspection window (chambers 15–18) is 86.4%. Therefore, it is comparable to the first. The bleeding here starts after 86 dimensionless residence times. The last inspection window (chambers 59–63) bleeds after 375 dimensionless residence times and loses 0.066 mL of stationary phase (81.2%).

The same trend of consecutive bleeding beginning next to the inlet and progressing toward the outlet over time is evident, but bleeding starts later than Arizona N. Therefore,

the critical minimal mean *Sf** of 0.256 (equaling *Sf* = 0.2) is reached after 317 dimensionless residence times—allowing for a prolonged operation.

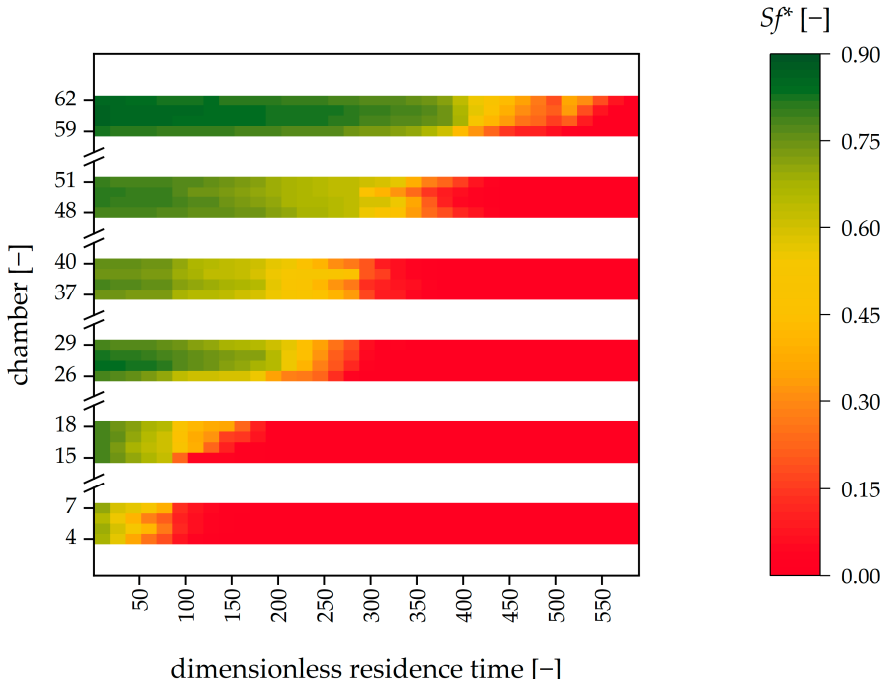

Figure 5. Retention values over time for the 6 viewing windows (containing 4 chamber–duct combinations each) of a transparent single-disc rotor. White areas indicate intransparent regions of the rotor. Phase system used: Arizona U, mobile phase flow: 15 mL·min^{-1}, 22 °C, 750 rpm, tripled runs.

The same behavior can be observed for the last system analyzed, Arizona G. As shown in Figure 6, the critical lower *Sf** is reached after 500 dimensionless residence times. Inspection window 4 loses 73.6% of the stationary phase after 135 dimensionless residence times. As mentioned in Chapter 3.1, the flow regime was kept constant. Therefore, the volumetric flow rate of the mobile phase was increased for Arizona G (20 mL·min^{-1}). The last inspection window starts to bleed after 692 dimensionless residence times. The loss of stationary phase here is 90.79%, the highest measured.

The different Arizona systems analyzed show varying bleeding rates and stability over time. With 500 dimensionless residence times, Arizona G is the most stable system. Arizona U reaches the critical lower *Sf* after 317 dimensionless residence times, whereas Arizona N is stable for only approximately 173 dimensionless residence times. Possible causes for this behavior could be the differing interfacial tensions (γ) combined with varying density differences ($\Delta\rho$) between the mobile and stationary phases. The same trend is apparent compared to the corresponding stability parameter α, which describes the hydrodynamic stability of a biphasic system in Countercurrent Centrifugal Chromatography [38].

$$\alpha = \frac{\gamma}{\Delta\rho} \tag{3}$$

The phase system Arizona G has the highest α of approximately 33 cm^3·s^{-2}, whereas Arizona N is prone to hydrodynamic instabilities with an α of only 17 cm^3·s^{-2}. Arizona U has an α of 27 cm^3·s^{-2}. With low values for α indicating small droplets being unstable and thus leading to emulsification and, therefore, destabilization of the phase, this trend corresponds to the experimental results discussed above [19].

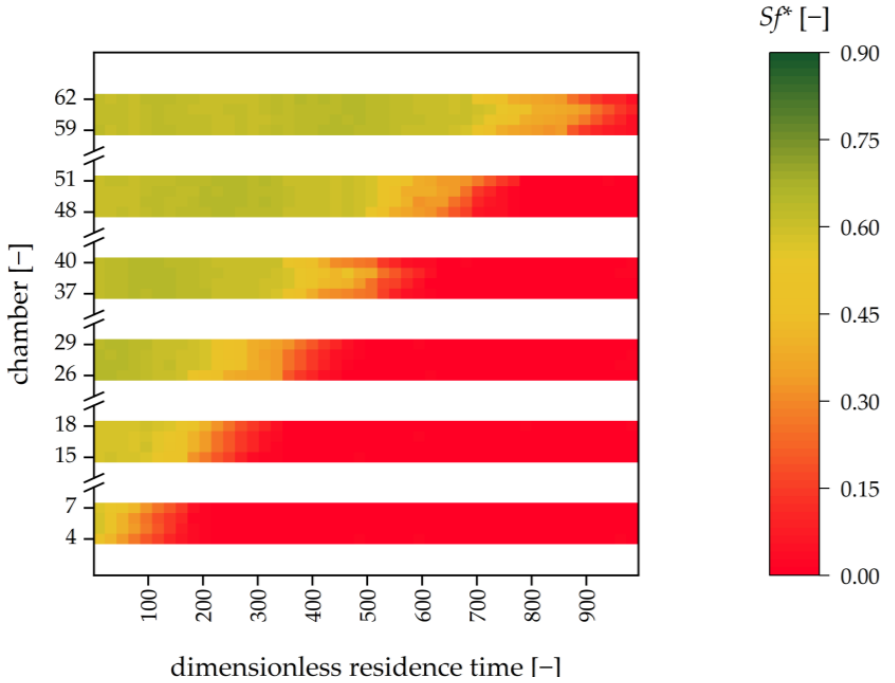

Figure 6. Retention values over time for the 6 viewing windows (containing 4 chamber–duct combinations each) of a transparent single-disc rotor. White areas indicate intransparent regions of the rotor. Phase system used: Arizona G, mobile phase flow: 20 mL·min^{-1}, 22 °C, 750 rpm, tripled runs, hydrodynamic residence time: 0.46 min.

Furthermore, the phase systems analyzed show different initial *Sf** before bleeding disturbs the hydrodynamic equilibrium in each chamber. For Arizona N, this approximately constant initial *Sf** is approximately 0.43 ± 0.06. For Arizona G, this value is 0.60 ± 0.05; for Arizona U, it is 0.77 ± 0.09.

3.3. Temperature Measurements

To estimate the energy input from the pumps and especially the rotary joints, fluid temperatures at the mobile phase outlet of the apparatus and the mobile phase tank were tracked for several retention experiments.

As can be seen in Figure 7, the mean temperature is 21.79 ± 0.01 °C (21.60 ± 0.01 °C in the tank) for Arizona N, for Arizona U it is 22.41 ± 0.01 °C (22.29 ± 0.01 °C in the tank), and for Arizona G the mean temperature is 22.10 ± 0.01 °C (22.11 ± 0.011 °C in the tank) at the outlet. The room temperature was 21.84 ± 1.13 °C—no significant shift in temperature is evident.

It can be stated that energy input caused by the equipment is compensated by heat transfer when the fluid passes uninsulated tubing. Shifts in room temperature mainly cause temperature differences between the different phase systems. In comparison, the outlet temperatures are always slightly higher than the tank temperatures. This is due to the positioning of the measurement location directly after the rotary joints, which likely contribute the most energy to the system. The risk that the miscibility gap of the phase system used will change because of a temperature shift during an experiment can be classified as low.

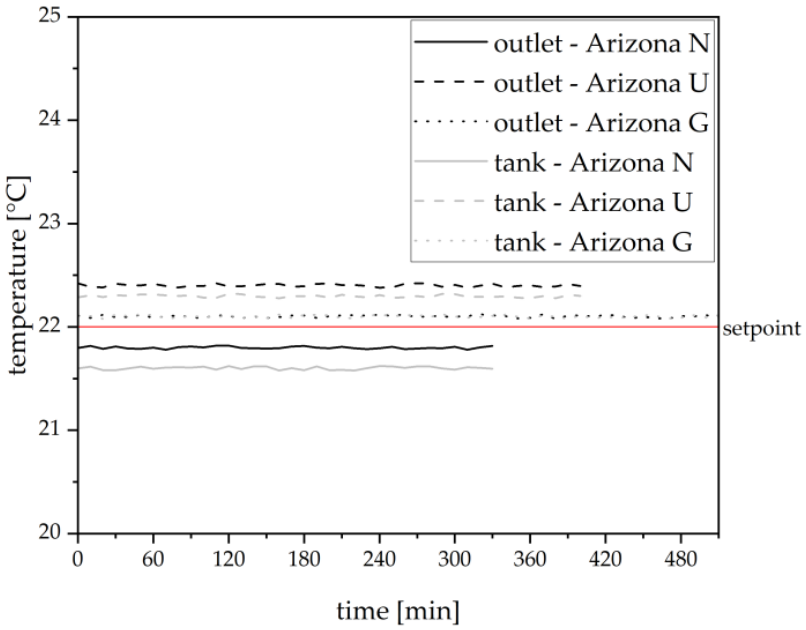

Figure 7. Temperature measurements of the mobile phase directly at the outlet of the apparatus and in the mobile phase storage tank (tempered) for different phase systems. The red line indicates the setpoint for the corresponding water bath.

4. Conclusions

In conclusion, this study presents significant experimental advancements and innovative insights into Liquid–Liquid Chromatography, with a particular focus on Centrifugal Partition Chromatography. With the help of a semi-transparent rotor and elevated image analysis automation, we were able to measure the loss of stationary phase not only timewise but also locally resolved. This novel approach provides unprecedented clarity and precision in monitoring the behavior of the stationary phase throughout the separation process. The results show an avalanche-like progression of bleeding starting at the inlet and progressing to the outlet over time. We could verify this behavior for different aqueous–organic phase systems and therefore analyzed the stability of Arizona systems with different polarities, which are crucial factors in Liquid–Liquid Chromatography.

Flow regime maps with varying volumetric flow rates of the mobile phase were generated beforehand to maintain comparable flow regimes throughout all experiments. In the next step, selecting those optimal volume flows that result in an equivalent flow regime was possible.

Finally, we measured temperatures inside the apparatus to track the energy input caused by the periphery. We disproved that energy input changes the equilibrium of the phase system significantly and thus might affect the bleeding observed.

Therefore, the risk of losing the stationary phase is present for Centrifugal Partition Chromatographs in general. This effect is accentuated differently depending on the operation parameters, the inner rotor geometry, and the phase system used. This bleeding directly influences separation efficiency, as discussed in Chapter 1. With decreasing amounts of stationary phase over time, the chromatographic resolution is also prone to drop. This would also result in suboptimal productivity of the plant. Separation tasks performed with the help of Centrifugal Partition Chromatography are often associated with constant phase ratios over time and are, therefore, potentially suboptimally operated [39–42].

This is why the knowledge gained contributes to the development of more efficient separation strategies and expands the scope of Liquid–Liquid Chromatography as a versatile separation technique. It has to be mentioned that different phase systems probably behave differently; when utilizing aqueous two-phase or deep eutectic solvent systems as liquid–liquid systems, their bleeding rates have to be measured individually [43].

In this context, it is advisable to consider the specific properties of the liquids used (i.e., when handling non-Newtonian fluids: shear-thinning will most likely behave differently to shear-thickening fluids in CPC) in a particular experiment and, if necessary, perform rheological tests.

In the next step, we will focus on developing solutions to counteract bleeding without disturbing the separation process. With this, our goal is to apply our innovative process control to the separation of complex mixtures (e.g., secondary metabolites from fermentation broth).

Author Contributions: Conceptualization, F.B., G.S. and J.K.; methodology, F.B.; software, F.B. and P.L.; experimental validation, P.L., D.H. and F.B.; formal analysis, P.L., D.H. and F.B.; investigation, P.L., D.H. and F.B.; data curation, F.B.; writing—original draft preparation, F.B.; writing—review and editing, F.B. and G.S.; visualization, F.B.; supervision, G.S. and J.K. All authors have read and agreed to the published version of the manuscript.

Funding: This research received no external funding.

Data Availability Statement: Data are contained within the article.

Conflicts of Interest: The authors declare no conflicts of interest.

Appendix A

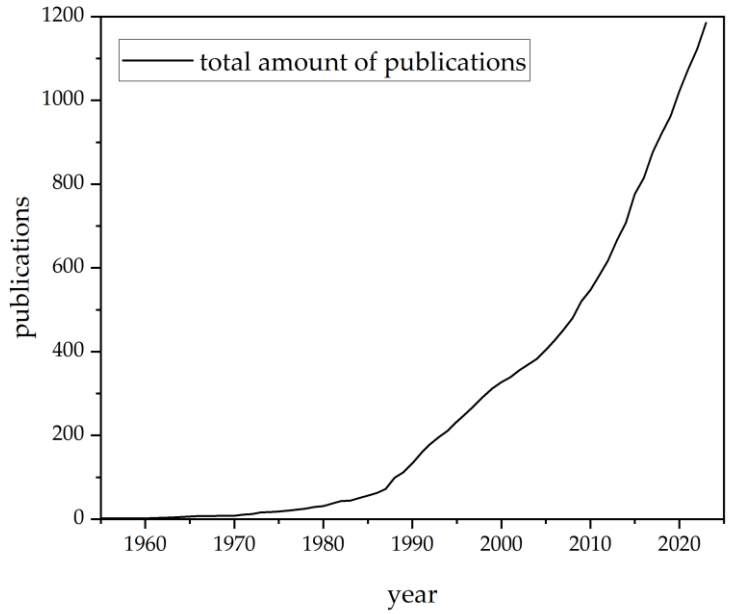

Figure A1. Total number of publications in the field of Countercurrent Chromatography. CPC was invented in 1982, and the growth in new publications per year increased.

Table A1. Physical properties for the Arizona systems used [35].

Arizona System	ρ_{UP} [g/cm^3]	ρ_{LP} [g/cm^3]	η_{UP} [mPa·s]	η_{LP} [mPa·s]	γ [mN/m]
G	0.85610 ± 0.0110	0.98433 ± 0.01189	0.42613 ± 0.00562	1.43356 ± 0.01727	4.25650 ± 0.56183
N	0.74838 ± 0.00224	0.92806 ± 0.01077	0.37546 ± 0.00171	1.46317 ± 0.00474	2.97165 ± 0.17757
U	0.69162 ± 0.00115	0.85470 ± 7.64992 × 10^{-4}	0.37547 ± 0.00142	0.99917 ± 0.00206	4.39761 ± 0.29576

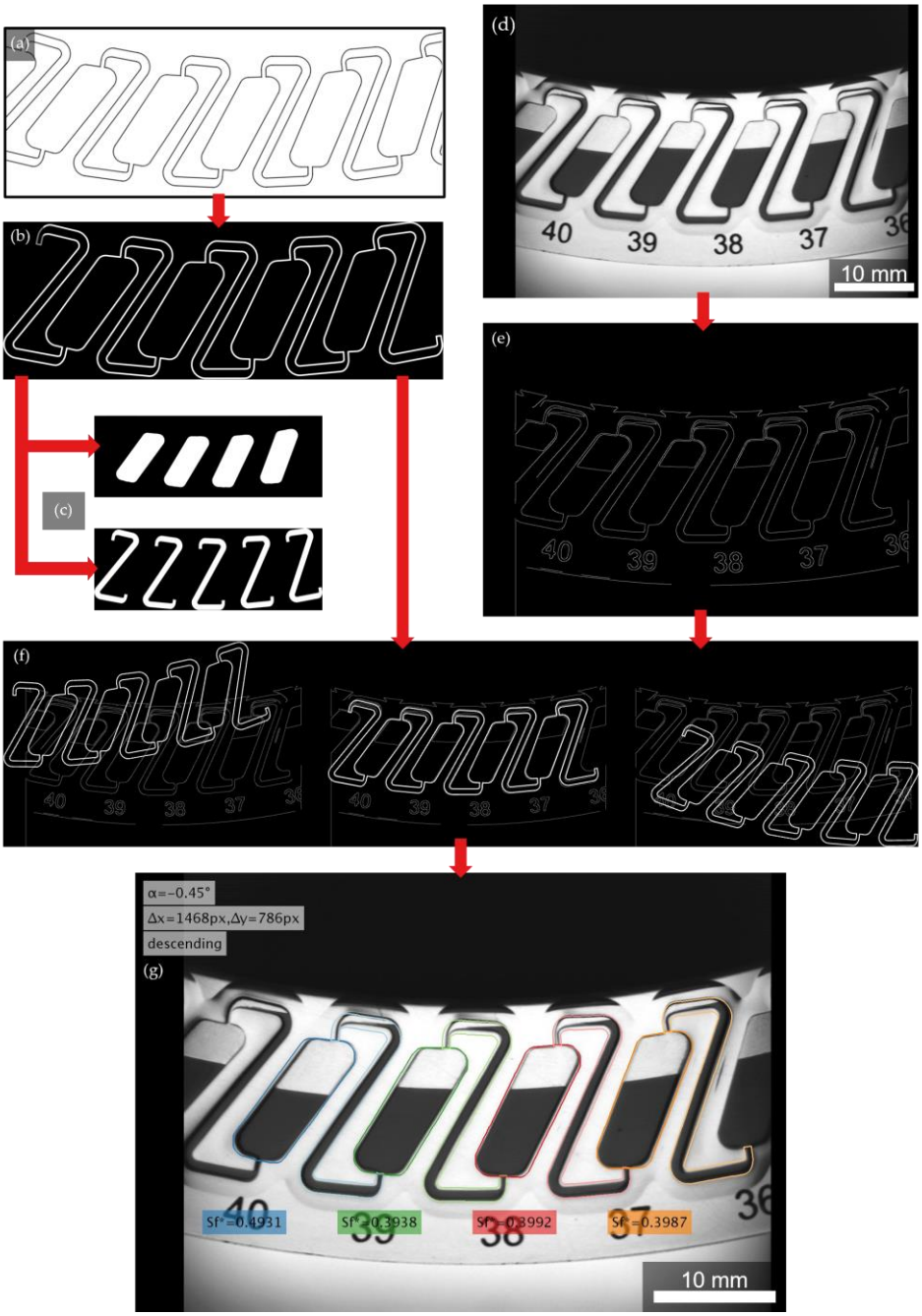

Figure A2. Flowchart of an image analysis process. (**a**) Rotor geometry in CAD software. (**b**) Generated template. (**c**) Chamber/channel areas delineating the image regions analyzed. (**d**) Extracted single frame from a video recording. (**e**) Edge detection result. (**f**) Iterative shift in x-y direction and rotation angle. (**g**) Result: reference image with recognized contour and calculated *Sf** values. (Phase system: Arizona G, rotational speed: 750 min^{-1}, mobile phase flow rate: 20 $mL \cdot min^{-1}$, measured after 10 min).

Figure A3. Flow regime map for Arizona N for volume flows of mobile phase between 2.5 mL·min^{-1} and 40 mL·min^{-1}. Measurement after 5 dimensionless residence times, 750 rpm, 22 °C.

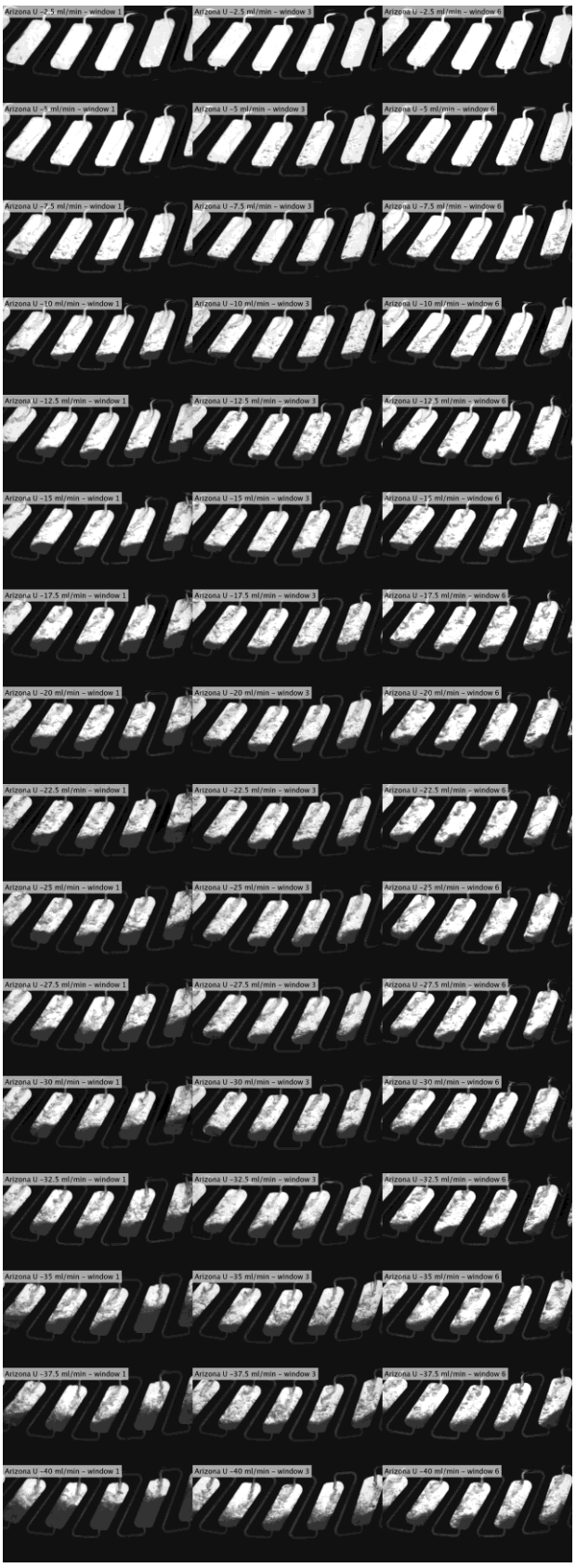

Figure A4. Flow regime map for Arizona U for volume flows of mobile phase between 2.5 mL·min^{-1} and 40 mL·min^{-1}. Measurement after 5 dimensionless residence times, 750 rpm, 22 °C.

Figure A5. Flow regime map for Arizona G for volume flows of mobile phase between 2.5 mL·min^{-1} and 40 mL·min^{-1}. Measurement after 5 dimensionless residence times, 750 rpm, 22 °C.

References

1. Friesen, J.B.; McAlpine, J.B.; Chen, S.-N.; Pauli, G.F. Countercurrent Separation of Natural Products: An Update. *J. Nat. Prod.* **2015**, *78*, 1765–1796. [CrossRef] [PubMed]
2. Bezold, F.; Goll, J.; Minceva, M. Study of the applicability of non-conventional aqueous two-phase systems in counter-current and centrifugal partition chromatography. *J. Chromatogr. A* **2015**, *1388*, 126–132. [CrossRef] [PubMed]
3. Gmehling, J.; Schedemann, A. Selection of Solvents or Solvent Mixtures for Liquid–Liquid Extraction Using Predictive Thermodynamic Models or Access to the Dortmund Data Bank. *Ind. Eng. Chem. Res.* **2014**, *53*, 17794–17805. [CrossRef]
4. Meucci, J.; Faure, K.; Mekaoui, N.; Berthod, A. Solvent Selection in Countercurrent Chromatography Using Small-Volume Hydrostatic Columns. *LCGC N. Am.* **2013**, *31*, 132–143.
5. Hopmann, E.; Frey, A.; Minceva, M. A priori selection of the mobile and stationary phase in centrifugal partition chromatography and counter-current chromatography. *J. Chromatogr. A* **2012**, *1238*, 68–76. [CrossRef] [PubMed]
6. Kostanian, A.E. Modelling counter-current chromatography: A chemical engineering perspective. *J. Chromatogr. A* **2002**, *973*, 39–46. [CrossRef] [PubMed]
7. Bezold, F.; Weinberger, M.E.; Minceva, M. Computational solvent system screening for the separation of tocopherols with centrifugal partition chromatography using deep eutectic solvent-based biphasic systems. *J. Chromatogr. A* **2017**, *1491*, 153–158. [CrossRef]
8. Frey, A.; Hopmann, E.; Minceva, M. Selection of Biphasic Liquid Systems in Liquid-Liquid Chromatography Using Predictive Thermodynamic Models. *Chem. Eng. Technol.* **2014**, *37*, 1663–1674. [CrossRef]
9. Marsden-Jones, S.; Colclough, N.; Garrard, I.; Sumner, N.; Ignatova, S. Using quantitative structure activity relationship models to predict an appropriate solvent system from a common solvent system family for countercurrent chromatography separation. *J. Chromatogr. A* **2015**, *1398*, 66–72. [CrossRef]
10. Ignatova, S.N.; Sutherland, I.A. A Fast, Effective Method of Characterizing New Phase Systems in CCC. *J. Liq. Chromatogr. Relat. Technol.* **2003**, *26*, 1551–1564. [CrossRef]
11. Wang, F.; Ito, Y.; Wei, Y. Recent progress on countercurrent chromatography modeling. *J. Liq. Chromatogr. Relat. Technol.* **2015**, *38*, 415–421. [CrossRef] [PubMed]
12. Ye, H.; Ignatova, S.; Peng, A.; Chen, L.; Sutherland, I. Optimising resolution for a preparative separation of Chinese herbal medicine using a surrogate model sample system. *J. Chromatogr. A* **2009**, *1216*, 5101–5105. [CrossRef] [PubMed]
13. Berthod, A. (Ed.) *Countercurrent Chromatography: The Support-Free Liquid Stationary Phase*; Elsevier: Amsterdam, The Netherlands, 2002; ISBN 9780444507372.
14. Buthmann, F.; Volpert, S.; Koop, J.; Schembecker, G. Prediction of Bleeding via Simulation of Hydrodynamics in Centrifugal Partition Chromatography. *Separations* **2024**, *11*, 16. [CrossRef]
15. Murayama, W.; Kobayashi, T.; Kosuge, Y.; Yano, H.; Nunogaki, Y.; Nunogaki, K. A new centrifugal counter-current chromatograph and its application. *J. Chromatogr. A* **1982**, *239*, 643–649. [CrossRef]
16. Fromme, A.; Fischer, C.; Keine, K.; Schembecker, G. Characterization and correlation of mobile phase dispersion of aqueous-organic solvent systems in centrifugal partition chromatography. *J. Chromatogr. A* **2020**, *1620*, 460990. [CrossRef]
17. Fromme, A.; Funke, F.; Merz, J.; Schembecker, G. Correlating physical properties of aqueous-organic solvent systems and stationary phase retention in a centrifugal partition chromatograph in descending mode. *J. Chromatogr. A* **2020**, *1615*, 460742. [CrossRef] [PubMed]
18. Adelmann, S.; Schembecker, G. Influence of physical properties and operating parameters on hydrodynamics in Centrifugal Partition Chromatography. *J. Chromatogr. A* **2011**, *1218*, 5401–5413. [CrossRef]
19. Fromme, A. Systematic Approach towards Solvent System Selection for Ideal Fluid Dynamics in Centrifugal Partition Chromatography. Ph.D. Dissertation, TU Dortmund University, Dortmund, Germany, 2020; ISBN 9783843916110.
20. Marchal, L.; Legrand, J.; Foucault, A. Mass transport and flow regimes in centrifugal partition chromatography. *AIChE J.* **2002**, *48*, 1692–1704. [CrossRef]
21. Marchal, L.; Foucault, A.; Patissier, G.; Rosant, J.M.; Legrand, J. Influence of flow patterns on chromatographic efficiency in centrifugal partition chromatography. *J. Chromatogr. A* **2000**, *869*, 339–352. [CrossRef]
22. Peng, A.; Hewitson, P.; Sutherland, I.; Chen, L.; Ignatova, S. The effect of increasing centrifugal acceleration/force and flow rate for varying column aspect ratios on separation efficiency in Counter-Current Chromatography. *J. Chromatogr. A* **2018**, *1581–1582*, 80–90. [CrossRef]
23. Ikehata, J.-I.; Shinomiya, K.; Kobayashi, K.; Ohshima, H.; Kitanaka, S.; Ito, Y. Effect of Coriolis force on counter-current chromatographic separation by centrifugal partition chromatography. *J. Chromatogr. A* **2004**, *1025*, 169–175. [CrossRef] [PubMed]
24. Popp, J.R.; Petrakis, E.A.; Angelis, A.; Halabalaki, M.; Bonn, G.K.; Stuppner, H.; Skaltsounis, L.A. Rapid isolation of acidic cannabinoids from Cannabis sativa L. using pH-zone-refining centrifugal partition chromatography. *J. Chromatogr. A* **2019**, *1599*, 196–202. [CrossRef] [PubMed]
25. Rutterschmidt, D.; Kovács, Z.; Lorantfy, L.; Misek, Z.; Rajsch, G. Taxol purification with Centrifugal Partition Chromatography. *Planta Med.* **2015**, *81*, PW_152. [CrossRef]
26. Fromme, A.; Fischer, C.; Klump, D.; Schembecker, G. Correlating the phase settling behavior of aqueous-organic solvent systems in a centrifugal partition chromatograph. *J. Chromatogr. A* **2020**, *1620*, 461005. [CrossRef] [PubMed]
27. Foucault, A.P. (Ed.) *Centrifugal Partition Chromatography*; Dekker: New York, NY, USA, 1995; ISBN 9780824792572.

28. Chollet, S.; Marchal, L.; Meucci, J.; Renault, J.-H.; Legrand, J.; Foucault, A. Methodology for optimally sized centrifugal partition chromatography columns. *J. Chromatogr. A* **2015**, *1388*, 174–183. [CrossRef] [PubMed]
29. Schwienheer, C.; Merz, J.; Schembecker, G. Investigation, comparison and design of chambers used in centrifugal partition chromatography on the basis of flow pattern and separation experiments. *J. Chromatogr. A* **2015**, *1390*, 39–49. [CrossRef] [PubMed]
30. Schwienheer, C. Advances in Centrifugal Purification Techniques for Separating (Bio-)chemical Compounds. Ph.D. Dissertation, TU Dortmund University, Dortmund, Germany, 2016; ISBN 9783843929165.
31. de La Poype, F.; de la Poype, R.; Durand, P.; Foucault, A.; Legrand, J.; Patissier, G.; Rosant, J.M. Cell Centrifuge Partition Chromatography Device. U. S. Patent No. 6537452, 25 March 2003.
32. Adelmann, S.; Schwienheer, C.; Schembecker, G. Multiphase flow modeling in centrifugal partition chromatography. *J. Chromatogr. A* **2011**, *1218*, 6092–6101. [CrossRef] [PubMed]
33. Krause, J.; Oeldorf, T.; Schembecker, G.; Merz, J. Enzymatic hydrolysis in an aqueous organic two-phase system using centrifugal partition chromatography. *J. Chromatogr. A* **2015**, *1391*, 72–79. [CrossRef] [PubMed]
34. Adelmann, S. On Hydrodynamics in Centrifugal Partition Chromatography. Ph.D. Dissertation, TU Dortmund University, Dortmund, Germany, 2014; ISBN 9783843916110.
35. Berthod, A.; Hassoun, M.; Ruiz-Angel, M.J. Alkane effect in the Arizona liquid systems used in countercurrent chromatography. *Anal. Bioanal. Chem.* **2005**, *383*, 327–340. [CrossRef] [PubMed]
36. Buthmann, F.; Pley, F.; Schembecker, G.; Koop, J. Automated Image Analysis for Retention Determination in Centrifugal Partition Chromatography. *Separations* **2022**, *9*, 358. [CrossRef]
37. van Buel, M.J.; van Halsema, F.E.D.; van der Wielen, L.A.M.; Luyben, K.C.A.M. Flow regimes in centrifugal partition chromatography. *AIChE J.* **1998**, *44*, 1356–1362. [CrossRef]
38. Foucault, A.P.; Frias, E.C.; Bordier, C.G.; Le Goffic, F. Centrifugal Partition Chromatography: Stability of Various Biphasic Systems and Pertinence of the "Stoke's Model" to Describe the Influence of the Centrifugal Field Upon the Efficiency. *J. Liq. Chromatogr.* **1994**, *17*, 1–17. [CrossRef]
39. Morley, R.; Minceva, M. Trapping multiple dual mode liquid-liquid chromatography: Preparative separation of nootkatone from a natural product extract. *J. Chromatogr. A* **2020**, *1625*, 461272. [CrossRef] [PubMed]
40. Marchal, L.; Intes, O.; Foucault, A.; Legrand, J.; Nuzillard, J.-M.; Renault, J.-H. Rational improvement of centrifugal partition chromatographic settings for the production of 5-n-alkylresorcinols from wheat bran lipid extract. *J. Chromatogr. A* **2003**, *1005*, 51–62. [CrossRef] [PubMed]
41. Bouju, E.; Berthod, A.; Faure, K. Carnosol purification. Scaling-up centrifugal partition chromatography separations. *J. Chromatogr. A* **2016**, *1466*, 59–66. [CrossRef]
42. Ward, D.P.; Hewitson, P.; Cárdenas-Fernández, M.; Hamley-Bennett, C.; Díaz-Rodríguez, A.; Douillet, N.; Adams, J.P.; Leak, D.J.; Ignatova, S.; Lye, G.J. Centrifugal partition chromatography in a biorefinery context: Optimisation and scale-up of monosaccharide fractionation from hydrolysed sugar beet pulp. *J. Chromatogr. A* **2017**, *1497*, 56–63. [CrossRef]
43. Bezold, F.; Minceva, M. A water-free solvent system containing an L-menthol-based deep eutectic solvent for centrifugal partition chromatography applications. *J. Chromatogr. A* **2019**, *1587*, 166–171. [CrossRef]